1-1-2007

Q2 dependence of the S11(1535) photocoupling and evidence for a P-wave resonance in η electroproduction

H. Denizli

Angela Biselli
Fairfield University, abiselli@fairfield.edu

CLAS Collaboration

Peer Reviewed

Published Citation

H. Denizli et al. [CLAS Collaboration], "Q2 dependence of the S11(1535) photocoupling and evidence for a P-wave resonance in η electroproduction", Physical Review C 76.1 (2007) DOI: 10.1103/PhysRevC.76.015204

Q^2 dependence of the $S_{11}(1535)$ photocoupling and evidence for a P-wave resonance in η electroproduction

H. Denizli,[1,32] J. Mueller,[32] S. Dytman,[32] M. L. Leber,[32] R. D. Levine,[32] J. Miles,[32] K. Y. Kim,[32] G. Adams,[33] M. J. Amaryan,[31] P. Ambrozewicz,[14] M. Anghinolfi,[20] B. Asavapibhop,[26] G. Asryan,[42] H. Avakian,[19,37] H. Bagdasaryan,[31] N. Baillie,[41] J. P. Ball,[3] N. A. Baltzell,[36] S. Barrow,[15] V. Batourine,[24] M. Battaglieri,[20] K. Beard,[23] I. Bedlinskiy,[22] M. Bektasoglu,[31,*] M. Bellis,[6] N. Benmouna,[16] N. Bianchi,[19] A. S. Biselli,[13,33] B. E. Bonner,[34] S. Bouchigny,[21,37] S. Boiarinov,[22,37] R. Bradford,[6] D. Branford,[12] W. J. Briscoe,[16] W. K. Brooks,[37] S. Bültmann,[31] V. D. Burkert,[37] C. Butuceanu,[41] J. R. Calarco,[28] S. L. Careccia,[31] D. S. Carman,[37] C. Cetina,[16] S. Chen,[15] P. L. Cole,[18,37] A. Coleman,[41,†] P. Collins,[3] P. Coltharp,[15] D. Cords,[37,‡] P. Corvisiero,[20] D. Crabb,[40] V. Crede,[15] J. P. Cummings,[33] N. Dashyan,[42] R. De Vita,[20] E. De Sanctis,[19] P. V. Degtyarenko,[37] L. Dennis,[15] A. Deur,[37] K. S. Dhuga,[16] R. Dickson,[6] C. Djalali,[36] G. E. Dodge,[31] J. Donnelly,[17] D. Doughty,[9,37] P. Dragovitsch,[15] M. Dugger,[3] O. P. Dzyubak,[36] H. Egiyan,[37,41,§] K. S. Egiyan,[42,‡] L. El Fassi,[2] L. Elouadrhiri,[9,37] A. Empl,[33] P. Eugenio,[15] L. Farhi,[8] R. Fatemi,[40] G. Fedotov,[27] G. Feldman,[16] R. J. Feuerbach,[6] T. A. Forest,[31] V. Frolov,[33] H. Funsten,[41] S. J. Gaff,[11] M. Garçon,[8] G. Gavalian,[31,42,§] G. P. Gilfoyle,[35] K. L. Giovanetti,[23] P. Girard,[36] F. X. Girod,[8] J. T. Goetz,[4] A. Gonenc,[14] R. W. Gothe,[36] K. A. Griffioen,[41] M. Guidal,[21] M. Guillo,[36] N. Guler,[31] L. Guo,[37] V. Gyurjyan,[37] K. Hafidi,[2] H. Hakobyan,[42] R. S. Hakobyan,[7] J. Hardie,[9,37] D. Heddle,[9,37] F. W. Hersman,[28] K. Hicks,[30] I. Hleiqawi,[30] M. Holtrop,[28] J. Hu,[33] C. E. Hyde-Wright,[31] Y. Ilieva,[16] D. G. Ireland,[17] B. S. Ishkhanov,[27] E. L. Isupov,[27] M. M. Ito,[37] D. Jenkins,[39] H. S. Jo,[21] K. Joo,[10,40] H. G. Juengst,[31] N. Kalantarians,[31] J. H. Kelley,[11] J. D. Kellie,[17] M. Khandaker,[29] K. Kim,[24] W. Kim,[24] A. Klein,[31] F. J. Klein,[7,37] M. Klusman,[33] M. Kossov,[22] L. H. Kramer,[14,37] V. Kubarovsky,[33] J. Kuhn,[6] S. E. Kuhn,[31] S. V. Kuleshov,[22] J. Lachniet,[31] J. M. Laget,[8,37] J. Langheinrich,[36] D. Lawrence,[26] K. Livingston,[17] H. Y. Lu,[36] K. Lukashin,[37,‖] M. MacCormick,[21] J. J. Manak,[37] N. Markov,[10] S. McAleer,[15] B. McKinnon,[17] J. W. C. McNabb,[6] B. A. Mecking,[37] M. D. Mestayer,[37] C. A. Meyer,[6] T. Mibe,[30] K. Mikhailov,[22] R. Minehart,[40] M. Mirazita,[19] R. Miskimen,[26] V. Mokeev,[27,37] K. Moriya,[6] S. A. Morrow,[8,21] M. Moteabbed,[14] V. Muccifora,[19] G. S. Mutchler,[34] P. Nadel-Turonski,[16] J. Napolitano,[33] R. Nasseripour,[36] S. O. Nelson,[11] S. Niccolai,[21] G. Niculescu,[23,30] I. Niculescu,[16,23] B. B. Niczyporuk,[37] M. R. Niroula,[31] R. A. Niyazov,[31,37] M. Nozar,[37] G. V. O'Rielly,[16] M. Osipenko,[20,27] A. I. Ostrovidov,[15] K. Park,[24] E. Pasyuk,[3] C. Paterson,[17] G. Peterson,[26] S. A. Philips,[16] J. Pierce,[40] N. Pivnyuk,[22] D. Pocanic,[40] O. Pogorelko,[22] E. Polli,[19] S. Pozdniakov,[22] B. M. Preedom,[36] J. W. Price,[5] Y. Prok,[40,¶] D. Protopopescu,[17] L. M. Qin,[31] B. A. Raue,[14,37] G. Riccardi,[15] G. Ricco,[20] M. Ripani,[20] B. G. Ritchie,[3] F. Ronchetti,[19] G. Rosner,[17] P. Rossi,[19] D. Rowntree,[25] P. D. Rubin,[35] F. Sabatié,[8,31] K. Sabourov,[11] J. Salamanca,[18] C. Salgado,[29] J. P. Santoro,[37,39,‖] V. Sapunenko,[20,37] R. A. Schumacher,[6] V. S. Serov,[22] A. Shafi,[16] Y. G. Sharabian,[37,42] J. Shaw,[26] N. V. Shvedunov,[27] S. Simionatto,[16,**] A. V. Skabelin,[25] E. S. Smith,[37] L. C. Smith,[40] D. I. Sober,[7] D. Sokhan,[12] M. Spraker,[11] A. Stavinsky,[22] S. S. Stepanyan,[24] S. Stepanyan,[37,42] B. E. Stokes,[15] P. Stoler,[33] I. I. Strakovsky,[16] S. Strauch,[36] M. Taiuti,[20] S. Taylor,[34] D. J. Tedeschi,[36] U. Thoma,[37,††] R. Thompson,[32] A. Tkabladze,[16,*] S. Tkachenko,[31] C. Tur,[36] M. Ungaro,[10] M. F. Vineyard,[35,38] A. V. Vlassov,[22] K. Wang,[40] D. P. Watts,[17,‡‡] L. B. Weinstein,[31] H. Weller,[11] D. P. Weygand,[37] M. Williams,[6] E. Wolin,[37] M. H. Wood,[36,§§] A. Yegneswaran,[37] J. Yun,[31] L. Zana,[28] J. Zhang,[31] B. Zhao,[10] and Z. W. Zhao[36]

(CLAS Collaboration)

[1]*Abant Izzet Baysal University, Bolu 14280, Turkey*
[2]*Argonne National Laboratory, Argonne, Illinois 60439, USA*
[3]*Arizona State University, Tempe, Arizona 85287-1504, USA*
[4]*University of California at Los Angeles, Los Angeles, California 90095-1547, USA*
[5]*California State University, Dominguez Hills, Carson, California 90747, USA*
[6]*Carnegie Mellon University, Pittsburgh, Pennsylvania 15213, USA*
[7]*Catholic University of America, Washington, DC 20064, USA*
[8]*CEA-Saclay, Service de Physique Nucléaire, F-91191 Gif-sur-Yvette, France*
[9]*Christopher Newport University, Newport News, Virginia 23606, USA*
[10]*University of Connecticut, Storrs, Connecticut 06269, USA*
[11]*Duke University, Durham, North Carolina 27708-0305, USA*
[12]*Edinburgh University, Edinburgh EH9 3JZ, United Kingdom*
[13]*Fairfield University, Fairfield, Connecticut 06824, USA*
[14]*Florida International University, Miami, Florida 33199, USA*
[15]*Florida State University, Tallahassee, Florida 32306, USA*
[16]*The George Washington University, Washington, DC 20052, USA*
[17]*University of Glasgow, Glasgow G12 8QQ, United Kingdom*
[18]*Idaho State University, Pocatello, Idaho 83209, USA*
[19]*INFN, Laboratori Nazionali di Frascati, I-00044 Frascati, Italy*
[20]*INFN, Sezione di Genova, I-16146 Genova, Italy*
[21]*Institut de Physique Nucleaire ORSAY, Orsay, France*
[22]*Institute of Theoretical and Experimental Physics, Moscow, 117259, Russia*

[23]*James Madison University, Harrisonburg, Virginia 22807, USA*
[24]*Kyungpook National University, Daegu 702-701, South Korea*
[25]*Massachusetts Institute of Technology, Cambridge, Massachusetts 02139-4307, USA*
[26]*University of Massachusetts, Amherst, Massachusetts 01003, USA*
[27]*Moscow State University, Skobeltsyn Nuclear Physics Institute, 119899 Moscow, Russia*
[28]*University of New Hampshire, Durham, New Hampshire 03824-3568, USA*
[29]*Norfolk State University, Norfolk, Virginia 23504, USA*
[30]*Ohio University, Athens, Ohio 45701, USA*
[31]*Old Dominion University, Norfolk, Virginia 23529, USA*
[32]*University of Pittsburgh, Pittsburgh, Pennsylvania 15260, USA*
[33]*Rensselaer Polytechnic Institute, Troy, New York 12180-3590, USA*
[34]*Rice University, Houston, Texas 77005-1892, USA*
[35]*University of Richmond, Richmond, Virginia 23173, USA*
[36]*University of South Carolina, Columbia, South Carolina 29208, USA*
[37]*Thomas Jefferson National Accelerator Facility, Newport News, Virginia 23606, USA*
[38]*Union College, Schenectady, New York 12308, USA*
[39]*Virginia Polytechnic Institute and State University, Blacksburg, Virginia 24061-0435, USA*
[40]*University of Virginia, Charlottesville, Virginia 22901, USA*
[41]*College of William and Mary, Williamsburg, Virginia 23187-8795, USA*
[42]*Yerevan Physics Institute, 375036 Yerevan, Armenia*
(Received 20 April 2007; published 27 July 2007)

New cross sections for the reaction $ep \to e'\eta p$ are reported for total center-of-mass energy $W = 1.5$–2.3 GeV and invariant squared momentum transfer $Q^2 = 0.13$–3.3 GeV^2. This large kinematic range allows the extraction of new information about response functions, photocouplings, and ηN coupling strengths of baryon resonances. A sharp structure is seen at $W \sim 1.7$ GeV. The shape of the differential cross section is indicative of the presence of a P-wave resonance that persists to high Q^2. Improved values are derived for the photocoupling amplitude for the $S_{11}(1535)$ resonance. The new data greatly expand the Q^2 range covered, and an interpretation of all data with a consistent parametrization is provided.

DOI: 10.1103/PhysRevC.76.015204 PACS number(s): 14.20.Gk, 13.30.Eg, 13.60.Le, 25.30.Rw

I. INTRODUCTION

Photoproduction and electroproduction experiments on the nucleon provide a clean probe of nucleon structure because quantum electrodynamics is well understood. As a result, the matrix elements for $\gamma N \to N^*, \Delta^*$ transitions, commonly called the photocoupling amplitudes, are sensitive to the nucleon and N^* quark-level wave function. These amplitudes have traditionally been calculated using quark models [1–3], but recently progress has been made in applying the techniques of lattice QCD [4–6]. Experimental measurements are currently being made of a number of different baryon resonances in several different final states. For a review of the current status, see Refs. [7,8].

Disentangling the wide and overlapping states that populate reaction data has been a long-lasting problem. In the mass region above the total center-of-mass (c.m.) energy W of 1.5 GeV, many overlapping baryon states are present, and some are not well known. The reaction $ep \to e'\eta p$ is especially clean, since processes involving ηN final states couple only to isospin $\frac{1}{2}$ resonances, simplifying the analysis. A prominent peak in the total cross section is seen for η production at $W = 1.535$ GeV in both γN and πN experiments. This is widely interpreted as the excitation of a *single* resonance, the spin $\frac{1}{2}$, negative parity, isospin $\frac{1}{2}$ state $S_{11}(1535)$ [9]. This state has a branching ratio to ηN of 45–60% compared to at most a few percent [9,10] for other states. This is a very interesting and unusual pattern.

η photoproduction experiments have reaffirmed the strong energy dependence and S-wave (isotropic) character close to threshold [11]. Using polarized photons [12], new values for ηN decay branching ratios of other resonances have been determined through interference with the dominant $S_{11}(1535)$.

*Current address: Ohio University, Athens, Ohio 45701, USA.
†Current address: Systems Planning and Analysis, Alexandria, Virginia 22311, USA.
‡Deceased.
§Current address: University of New Hampshire, Durham, New Hampshire 03824-3568, USA.
‖Current address: Catholic University of America, Washington, D.C. 20064, USA.
¶Current address: Massachusetts Institute of Technology, Cambridge, Massachusetts 02139-4307, USA.
**Current address: San Paulo University, Brazil.
††Current address: Physikalisches Institut der Universitaet Giessen, D-35392 Giessen, Germany.
‡‡Current address: Edinburgh University, Edinburgh EH9 3JZ, United Kingdom.
§§Current address: University of Massachusetts, Amherst, Massachusetts 01003, USA.

Electroproduction cross sections can be used to extract the photocoupling amplitude for nonzero values of the squared momentum transfer Q^2 from the electron to the resonance. Using η electroproduction [13–19], an unusually flat Q^2 dependence of the photocoupling amplitude was found for the $S_{11}(1535)$ in contrast to the nucleon form factors and photon coupling amplitudes of other established resonances, e.g., $P_{33}(1232)$ [20]. Although previous η angular distributions were largely isotropic at all Q^2, no detailed response functions were extracted because of the poor angular coverage using traditional magnetic spectrometers. Although the Q^2 dependence was clearly different than for other resonances, the results were comprised of many different experiments whose results appeared to be inconsistent with each other. An analysis by Armstrong *et al*. [19] showed that much of the inconsistency was due to different assumptions about $S_{11}(1535)$ properties used by the individual experiments.

In our previous publication [21], we presented results on η electroproduction based on the first data taken with the Continuous Electron Beam Accelerator Facility (CEBAF) Large Acceptance Spectrometer (CLAS) [22] at Jefferson Lab. We extracted the photocoupling amplitude $A_{\frac{1}{2}}$ for the $S_{11}(1535)$ over the range $0.25 < Q^2 < 1.5$ GeV^2 from our data. In addition, we observed the indication of a structure at $W \approx 1.7$ GeV in the total cross section which is also seen as a change in the shape of the differential cross section at the same energy.

The energy region around $W \approx 1.7$ GeV has received significant attention lately. At the same energy, a CLAS $\pi^+\pi^-$ electroproduction experiment [23] found excess strength beyond theoretical predictions based on previous data. This excess strength was tentatively identified as a P-wave resonance; either the decay properties of $P_{13}(1720)$ change significantly or there is a new spin $\frac{3}{2}^+$ state. A recent η photoproduction experiment at Bonn [24] provides a comprehensive set of cross section data from near threshold to well beyond the resonance region. In the same paper [24], a partial wave analysis of these and other η electroproduction data finds strong excitation of a $J = 3/2^+$ state at 1775 MeV which they identify with the $P_{13}(1720)$. Although previous analyses [9] found weak evidence for any ηN decay of resonances at $W \sim 1.7$ GeV, the new data is of much higher quality than the older data.

The data and analysis reported here use a data set taken with the same apparatus (CLAS) as used in our first publication [21]. The new data have an order of magnitude more η events than in that previous paper and a much larger kinematic range. Therefore, the new values presented here supersede the previously published data. Our reach in Q^2 (0.13–3.3 GeV^2) is more than twice as large as in our first publication. This allows a large extension of the Q^2 range where we can extract the photocoupling amplitude $A_{\frac{1}{2}}$ of the proton to $S_{11}(1535)$ transition. We also more precisely determine the nonisotropies in the differential cross section and show evidence for a significant contribution to η electroproduction due to a P-wave resonance with a mass around 1.7 GeV.

The paper first presents some formalism needed to understand the measurement and its analysis, followed by details of the experiment. We then present results for the inclusive and exclusive analyses. Discussion of these results with a Breit-Wigner model and conclusions complete the paper.

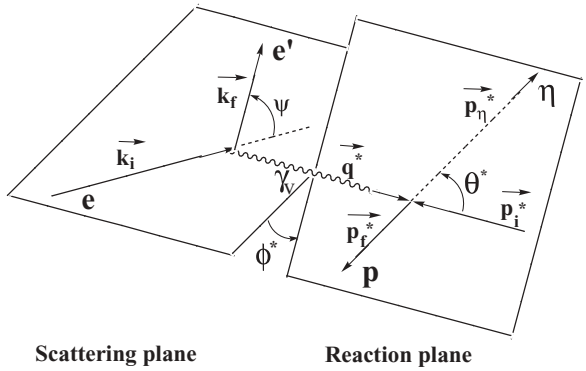

FIG. 1. The reaction is depicted in the c.m. system, where the resonance is at rest. The meson decay polar angle is defined relative to the virtual photon momentum, and the azimuthal angle is defined relative to the the electron scattering plane.

II. FORMALISM

The kinematics for the $ep \to e'\eta p$ reaction are shown in Fig. 1. It can be characterized in terms of the squared four-momentum transfer between the electron and proton $(-Q^2)$ carried by the virtual photon (γ_v), the invariant mass of the γ_v-p system (W), and the scattering angles of the final state η in the rest frame of the γ_v-p system (θ^*, ϕ^*). These angles are also the decay angles of the resonance in its rest frame. We use the superscript $*$ for quantities evaluated in this frame. The fivefold unpolarized differential cross section for the $ep \to e'\eta p$ process at a specific energy E may be expressed as the product of the transverse virtual photon flux Γ_γ in the Hand convention [25] and the c.m. cross section for virtual photoproduction of the $p\eta$ pair:

$$\frac{d^5\sigma}{dW\,dQ^2\,d\Omega_\eta^*} = \Gamma_\gamma(E, W, Q^2)\frac{d^2\sigma}{d\Omega_\eta^*}(\gamma_v p \longrightarrow \eta p). \quad (1)$$

The cross section for the virtual reaction $\gamma_v p \longrightarrow \eta p$ is written by convention to explicitly display the dependence on ϕ^*, that is,

$$\frac{d^2\sigma}{d\Omega_\eta^*}(\gamma_v p \longrightarrow \eta p) = \sigma_T + \epsilon\sigma_L + \sqrt{2\epsilon(1+\epsilon)}\sigma_{LT}\cos\phi_\eta^* + \epsilon\sigma_{TT}\cos 2\phi_\eta^*, \quad (2)$$

where ϵ is the longitudinal degree of polarization of the virtual photon and is given by

$$\epsilon = \left[1 + 2\left(1 + \frac{q^2}{Q^2}\right)\tan^2\left(\frac{\Psi}{2}\right)\right]^{-1}, \quad (3)$$

where q is the magnitude of the three-momentum of the virtual photon and Ψ is the electron scattering angle. Since ϵ is invariant under collinear transformations, q and Ψ may be expressed either in the laboratory or c.m. frame. The component cross sections can be expressed in terms that are

related to the spin of the photon and target, very similar to the definition of response functions [8]. In an unpolarized experiment, there are four independent terms. The cross sections for transverse and longitudinal photons are represented by σ_T and σ_L, respectively. In addition, σ_{LT} is a contribution due to the interference between transverse and longitudinal amplitudes, and σ_{TT} describes the interference between amplitudes for the two different transverse polarizations, either aligned or anti-aligned with the spin of the target proton. All four of these terms depend on W, Q^2, and $\cos\theta^*$.

To identify individual baryon resonances, the cross section should be decomposed into partial wave amplitudes. These amplitudes are most often labeled by the electromagnetic multipole notation [26]. Multipoles are commonly labeled $E_{l\pm}$, $M_{l\pm}$, and $S_{l\pm}$, where l is the orbital angular momentum of the final ηp system and $\pm$ denotes whether the total angular momentum is $l \pm \frac{1}{2}$. E and M refer to electric and magnetic transitions involving transverse virtual photons, while the longitudinal S transitions involve longitudinal photons.

The response functions and multipoles have contributions from underlying resonant and nonresonant reaction mechanisms. When evaluated at the peak of the resonance, the multipole is expressed in terms of both the photocoupling amplitude and the hadronic decay properties of the individual resonances in a commonly accepted way [27]. The photocoupling amplitudes are labeled by the γN total helicity ($\frac{1}{2}$ or $\frac{3}{2}$) and the virtual photon polarization (transverse or longitudinal) and depend on the invariant squared momentum transfer to the resonance (Q^2). The shape of the resonance determines the W dependence of the resonant part of the multipole. Spin-$\frac{1}{2}$ resonances will be described by one transverse amplitude $A_{\frac{1}{2}}$ and one longitudinal amplitude $S_{\frac{1}{2}}$. In terms of multipoles, an S_{11} resonance has an E_{0+} (electric dipole) and an S_{0+} transition; a P_{11} has M_{1-} and S_{1-} transitions. Higher spin resonances will be described by both $A_{\frac{1}{2}}$ and $A_{\frac{3}{2}}$ photocouplings (and both E and M multipoles). Extraction of the multipole amplitudes from the cross section data, see, e.g., [28], is not unique, because more than one bilinear combination of multipoles have identical angular distributions. We therefore choose simplified methods (discussed below) to analyze the data.

The differential cross sections can be calculated with a model of resonance production/decay and the nonresonant processes. This cannot yet be done from a fundamental field theory such as quantum chromodynamics (QCD). Instead, models are used that have parameters determined from data. The η-MAID [29] model uses an isobar model [30] to construct the cross section for η photo- and electroproduction; parameters are fit by comparisons with previous results [11,21,31]. We have calculations from the MAID code for our kinematics. To further understand our data, we also do Legendre polynomial fits to the angular distributions. Both these results are described in Sec. IV B.

To analyze our angle-integrated cross sections, we make a further simplification which is possible because the $S_{11}(1535)$ resonance is dominant near threshold. Therefore, we ignore the nonresonant amplitude. If one can isolate the contribution of a single S_{11} resonance to the E_{0+} multipole, the cross section takes the simple form

$$\frac{d\sigma}{d\Omega_\eta^*} = \frac{p_\eta^* W}{m_p K} |E_{0+}(W)|^2, \tag{4}$$

where $K = (W^2 - m_p^2)/(2m_p)$ is the equivalent real photon energy, p_η^* is the momentum of the outgoing η in the S_{11} rest frame, and m_p is the proton mass. The longitudinal multipole S_{0+} does, in principal, contribute, and we do not have the data to make the separation. However, S_{0+} has been found to be small [17], and it was therefore ignored in previous analyses [11,13,14,16–19,21]. An isobar model analysis of ηp, $\pi^0 p$, and $\pi^+ n$ CLAS electroproduction data [32] confirms the assumption of a small longitudinal component. In this analysis, the value of $S_{\frac{1}{2}}/A_{\frac{1}{2}}$ is about 15–20%; this translates to a few percent contribution to the cross sections measured here. With the assumption that a single resonance dominates the cross section and $S_{\frac{1}{2}}$ is small, $A_{\frac{1}{2}}$ for $\gamma p \to S_{11}(1535)$ can be determined from Ref. [27] as

$$A_{\frac{1}{2}} = \sqrt{2\pi \frac{p_\eta^* W_R^2 \Gamma_R}{K m_p^2 b_\eta}} \mathrm{Im}(E_{0+}(W_R)), \tag{5}$$

where E_{0+} refers only to the contribution from the resonance which is evaluated at the peak of the resonance. If there are other contributions to E_{0+}, a model is needed to extract the resonance contribution. This formula contains terms related to the final state decay of the S_{11}: Γ_R, the total width of the $S_{11}(1535)$; b_η, the branching fraction into the ηp final state; and p_η^* are all calculated at the mass of the S_{11} (W_R). Our current lack of knowledge of these parameters leads to a model dependence in the extracted values for $A_{\frac{1}{2}}$. This prompted Benmerrouche *et al.* [33] to propose using a quantity for each resonance with less model dependence, that is,

$$\xi_{\frac{1}{2}} = \sqrt{\frac{m_p^2 K b_\eta}{W_R^2 p_\eta^* \Gamma_R}} A_{\frac{1}{2}}. \tag{6}$$

$A_{\frac{1}{2}}$ depends on the matrix element for the initial state $\gamma N \to N^*$ transition, while $\xi_{\frac{1}{2}}$ is proportional to the product of the matrix elements for the $\gamma N \to N^*$ and $N^* \to \eta p$ transition. For $S_{11}(1535)$, $\xi_{\frac{1}{2}} = \sqrt{2\pi}\mathrm{Im}(E_{0+}(W_R))$. Although $\xi_{\frac{1}{2}}$ is more closely related to experimental values, $A_{\frac{1}{2}}$ is more easily determined from calculations, e.g., using quark models. Whichever quantity is used, the model dependence still exists when comparing calculations to experiment.

We use the same resonance parametrization in all our calculations. The relativistic Breit-Wigner form is taken from previous η photoproduction work [34,35] and extended to nonzero angular momentum as

$$\frac{d\sigma_{\mathrm{BW}}}{d\Omega_\eta^*}(W) = \frac{p_\eta^*}{q^*} \left| T_{\mathrm{BW}}^\ell(W) \right|^2, \tag{7}$$

$$T_{\mathrm{BW}}^\ell(W) = \frac{a W_R \Gamma_\eta}{\left(W_R^2 - W^2\right) - i W_R \Gamma_{\mathrm{tot}}}, \tag{8}$$

where a is a constant that contains the photocoupling amplitude and kinematic factors, q^* is the photon three-momentum in the resonance rest frame, Γ_η is the partial width for

TABLE I. Summary of kinematic ranges of previously published data compared with this experiment. This experiment is an extension of Ref. [21]. Values given are the maximum ranges for each experiment.

Experiments	W (GeV)	Q^2 (GeV^2)	$\cos\theta^*$	ϕ^* (deg)
Daresbury [13]	1.51 → 1.55	0.15 → 1.5	not given	not given
Bonn [14]	1.51 → 1.56	0.2 → 0.4	−0.766 → 0.939	∼0
DESY [15]	1.5 → 1.7	0.22 → 1.0	−1 → 1	0 → 180
DESY [16]	1.49 → 1.58	0.6, 1.0	−1 → 1	15 → 90
Bonn [17]	1.44 → 1.64	0.4	−0.643 → 0.866	−40 → 40
DESY [18]	1.49 → 1.8	2.0, 3.0	−1 → 1	0 → 120
JLab [19]	1.48 → 1.62	2.4, 3.6	−1 → 1	0 → 360
JLab [21]	1.5 → 1.86	0.375 → 1.5	−1 → 1	0 → 360
This experiment	1.5 → 2.3	0.13 → 3.3	−1 → 1	0 → 360

$N^* \to \eta p$ decay, and $\Gamma_{\rm tot}$ is the total width,

$$\Gamma_\eta = \frac{B_\ell(p^*_\eta)}{B_\ell(p^*_{\eta,R})}\Gamma_R, \tag{9}$$

$$\Gamma_{\rm tot} = \left(0.5\frac{p^*_\eta}{p^*_{\eta,R}}\frac{B_\ell(p^*_\eta)}{B_\ell(p^*_{\eta,R})} + 0.4\frac{p^*_\pi}{p^*_{\pi,R}}\frac{B_\ell(p^*_\pi)}{B_\ell(p^*_{\pi,R})} + 0.1\right)\Gamma_R, \tag{10}$$

where Γ_R is the bare width and $B_\ell(p^*)$ is a Blatt-Weisskopf penetration factor [36]. If $\ell = 0$, this factor is equal to unity. The momentum ratios [35] approximately account for proper phase space effects for the various final states (πN, ηN, and $\pi\pi N$, where the phase space factors for the $\pi\pi N$ final state are ignored). They are weighted according to estimates of the branching fractions to each final state. This form has been successful in matching data but is not unique.

III. DETECTOR AND ANALYSIS

The CLAS facility [22] was designed for the efficient detection of multiparticle final states. The data used for this measurement were taken in 1999 at electron beam energies of 1.5, 2.5, and 4.0 GeV. A cylinder of liquid hydrogen was used as the target. Two different targets were used, 5.0 and 3.8 cm long. Toroidal magnet coils separate CLAS into six largely identical sectors, each covering roughly 54° in azimuthal angle ϕ (with smaller coverage at smaller polar angle). Tracking drift chambers (DCs) in CLAS measure angles and momenta of charged particles for laboratory polar angles in the range $8^\circ < \theta < 142^\circ$. Outside the DCs, scintillation counters (SCs) provide time-of-flight measurements with which we can separate the charged hadrons into pions, kaons, and protons. For laboratory angles $\theta < 48^\circ$, threshold Cherenkov counters (CCs) and electromagnetic calorimeters (ECs) distinguish electrons from charged hadrons.

For this analysis, events were selected with an identified electron and proton. Since the momentum four-vectors of the beam and target are known, the four-vector for the putative η can be determined from these two final state particles. A fiducial cut on these particles was applied to avoid the regions near the magnetic coils and the edges of the CC where the acceptance is changing rapidly. The momentum of the electron was required to be above 400 MeV in order to be well above the trigger threshold.

Cross sections were calculated as a function of Q^2 and W for the angle-integrated data analysis and as a function of Q^2, W, $\cos\theta^*$, and ϕ^* for the differential data analysis. Cross sections are determined in a standard way by determining the yield in each of many bins, correcting for detector acceptance, and normalizing by the beam intensity measured with a Faraday cup and the calculated target thickness.

As discussed in Sec. II, the extraction of resonance properties comes from an analysis of the $\cos\theta^*$, ϕ^* distributions at specific values of W and Q^2. Distributions of these variables covered by the apparatus are determined by geometry. The large acceptance of CLAS guarantees almost complete coverage in $\cos\theta^*$ and ϕ^*. The beam energies of the experiment coupled with CLAS provided data at a wide range of Q^2 and W. We compare the kinematic range for the new experiment with that available for the previously published η electroproduction data in Table I.

Events were divided into separate kinematic bins as detailed in Sec. IV. For each bin, the η yield was determined by fitting the distribution of missing mass recoiling against the outgoing e-p system. An example fit in one bin is shown in Fig. 2.

The fit is the sum of a signal at the η mass and a background function. The signal shape has a radiative tail and is corrected for experimental resolution; the background function is a polynomial. We use the data to determine both shapes. Both functions must then be modified by the geometric acceptance for this reaction, because it has a rapid variation with respect to the kinematic parameters. This method is an extension of what was used in the previous CLAS data analysis [21].

The shape of the signal was modeled in two steps to reproduce all features seen in the data. It is first described by a δ function at the η mass (m_η) plus an exponential above m_η representing the radiative tail,

$$S(m) = (1-f)\delta(m-m_\eta) + f\Theta(m-m_\eta)e^{-\alpha(m-m_\eta)}.$$

The fraction of events in the radiative tail (f) and a parameter describing the slope in the exponential (α) were determined for each W-Q^2 bin from Monte Carlo generator events containing radiative effects [37,38]. This signal shape was then convoluted with a Gaussian representing the experimental resolution to obtain the final signal shape (an analytic function) used to fit

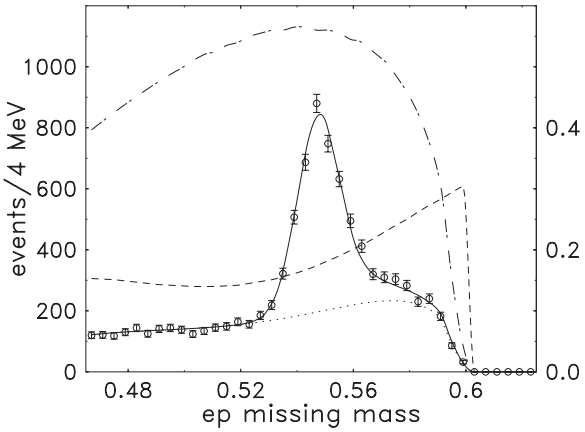

FIG. 2. Sample missing mass M_X spectrum for $ep \to epX$. The bin shown is for $W = 1.535$ GeV and $Q^2 = 0.6$ GeV^2. The dashed line (right scale) shows the acceptance that is calculated with a Monte Carlo program. The sum of the η signal shape and the raw background function modified by the acceptance function is then fit to the missing mass spectrum for each bin. In the figure, the dot-dashed curve is the raw background function $D_{\rm bkg}$ from this fit, while the dotted curve shows those same values when multiplied by the acceptance function. The solid curve shows the full fit.

for the η yield. In the fit to obtain the yields, only the magnitude of the signal and background functions were free. All other parameters were determined separately. The rms resolution for the missing mass peak ranged from 4 MeV in the low Q^2 bins up to 12 MeV at the highest Q^2. The experimental η mass, experimental resolution width, f, and α were first fit to simple functions of Q^2 and W for both data and Monte Carlo to smooth out statistical variations. The experimental η mass was found to be within 1 MeV of the accepted value. Estimated contributions to the systematic uncertainty by these choices of parameters were evaluated in a later step.

The background comes from $\pi\pi$ production. Although it has a smooth dependence on M_X, no models are available. We fit the background with a simple polynomial $D_{\rm bkg}$ in the missing mass M_X constrained to be zero at the kinematic limit $m_{\rm max}$ as required by the decreasing phase space, such that

$$D_{\rm bkg}(M_X) = b_0(2\sqrt{\Delta m' \Delta m} - \Delta m), \qquad (11)$$

where $\Delta m = m_{\rm max} - M_X$ and b_0 is the overall strength. One example of this function is shown in Fig. 2. At the highest beam energy, a slightly more complicated function was used. Both forms contained one parameter ($\Delta m'$) that was determined from our data by fitting to a polynomial in W. As with the peak shape function parameters, these fit parameters were included in the systematic uncertainty determination.

The main structure in the background fit function comes from the variation of the geometric acceptance of the detector as a function of missing mass. We found that proper modeling of this acceptance was very important. We determined this acceptance using a separate Monte Carlo program that generated $ep \to epX$ events with the X mass thrown randomly across the fit region. After requiring the scattered electron and proton to be in the fiducial volume of CLAS, we compared the generated and accepted events in order to calculate the background acceptance function. We multiply our simple background function with the calculated acceptance function to obtain the final background used in the fit. Examples of all three of these curves are shown in Fig. 2.

In a small number of bins where the cross section is low, statistical fluctuations in the background can lead to a best-fit value for the number of η's that is negative. In this case, we follow the suggestion of the Particle Data Group (PDG) [9] and report a negative value with error bars for the cross section. This provides sufficient information for constraints from these bins to be combined with nearby bins in comparing with theoretical predictions.

Acceptance for the $ep \to e\eta p$ reaction was calculated using a GEANT-based Monte Carlo simulation [39]. The event generator included radiative effects using the peaking approximation [37,38], and the cross sections have been corrected for radiation. When making a major improvement in published cross sections, development of an appropriate event generator is important. We use the data as a guide; the final cross section is dominated by S and P waves with the $S_{11}(1535)$ the dominant structure seen. An iterative procedure matching analyzed Monte Carlo to real data was used to develop the event generator. The same fitting procedure used on data was applied to Monte Carlo events to calculate acceptance. The acceptance has significant variation across the bins with a maximum value of about 60%. When approaching the kinematic limit, the acceptance falls off rapidly. At the higher values of W, the proton goes forward where there is a hole in the CLAS acceptance. This causes problems for $\phi_\eta \sim 180^\circ$. We only report results in bins where the acceptance is greater than 3% and where it is not changing rapidly.

A detailed study of potential sources of systematic uncertainty was made. Since the η peak shape and the background shape included various parameters, all were studied. The parameters were varied within the error bars determined in the fit for each cross section value. Additional tests were made for variations in particle identification and in the momentum scale. The momentum uncertainty arose from uncertainty in the details of both the magnetic field map and the alignments of the various tracking chambers. Sensitivity to momentum determination was largest close to threshold and falls off with increasing W. Since most of the η events are produced near threshold, this source dominates the average systematic uncertainty. Cross sections were recalculated with slightly tighter fiducial cuts, and this variation was considered as a systematic uncertainty estimate. A variety of underlying physics models were used for evaluating the systematic on the radiative correction: using a single S-wave resonance or two, varying the mass and width of a single S wave, or including a P-wave resonance. The quoted systematic uncertainty on the radiative correction includes these effects, but is dominated by Monte Carlo statistics in the calculation. The total systematic uncertainty for each bin in W, Q^2, and c.m. scattering angles was the sum of all the components added in quadrature. The average total systematic uncertainty for the angle-integrated cross sections was 3.3%, 3.9%, and 7.1% for data at 1.5, 2.5, and 4.0 GeV, respectively. The corresponding average estimated systematic uncertainties for the differential cross sections were 5.1%, 5.2%, and 7.6%. The breakdown by source

TABLE II. Summary of systematic uncertainties for the angle-integrated and differential cross section analysis. M_η, σ_η, f, α, and "radiative corr." describe the η missing mass peak shape; $D_{\rm bkg}$ is the background missing mass function; other entries parametrize various detector properties. See text for details.

Sys error source	Angle-integrated (int)	Differential (diff)
M_η	0.03%	0.06%
σ_η	0.4%	0.7%
f	1.3%	1.4%
α	0.1%	0.1%
$D_{\rm bkg}(M_X)$	0.1%	0.1%
Fiducial cut	0.6%	2.3%
Radiative corr.	1.0%	1.0%
Momentum scale	2.6%	4.4%
Total	3.9%	5.2%

for the 2.5 GeV data (the set from which the largest number of data points come) is given in Table II. The estimated systematic uncertainties for individual data points were seldom larger than the estimated statistical uncertainty.

IV. RESULTS

A. Angle-integrated cross sections

To get the angle-integrated cross sections, the events were binned in W and Q^2, as shown in Table III. The 1.5 GeV beam energy data cover the Q^2 range from 0.13 to 0.4 GeV^2, while the upper two beam energies cover 0.6–3.3 GeV^2. Each bin is labeled by its centroid. Results are tabulated in the CLAS database [40]. These cross sections are presented in Fig. 3. The prominent peak at $W \sim 1.5$ GeV is primarily populated through intermediate excitation of the $S_{11}(1535)$ resonance. Fits to a Breit-Wigner relativistic form with an energy-dependent width, Eq. (8), are used to fit the low W region. Various model calculations [33] in the past have found

TABLE III. Binning details for the angle-integrated cross sections. For each Q^2 bin, we show the minimum and maximum values of Q^2, the energy of the electron beam for the data set, and the maximum value of W probed. The W bin width in all cases was 10 MeV.

$Q^2_{\rm min}$ (GeV^2)	$Q^2_{\rm max}$ (GeV^2)	$E_{\rm beam}$ (GeV)	$W_{\rm max}$ (GeV)
0.13	0.2	1.5	1.66
0.2	0.3	1.5	1.64
0.3	0.4	1.5	1.61
0.6	0.8	2.5	2.00
0.8	1.0	2.5	1.90
1.0	1.2	2.5	1.81
1.2	1.4	2.5	1.69
1.3	1.7	4.0	2.30
1.7	2.1	4.0	2.30
2.1	2.5	4.0	2.13
2.5	2.9	4.0	1.93
2.9	3.3	4.0	1.72

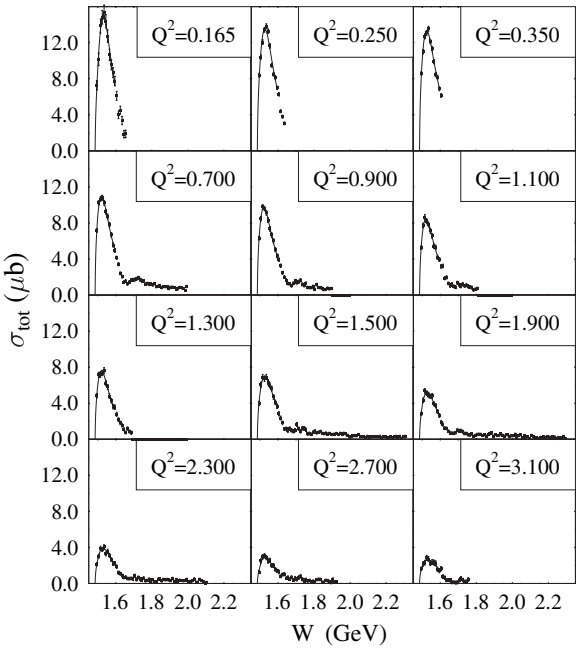

FIG. 3. Angle-integrated cross sections $\sigma(\gamma_v p \to \eta p)$ measured in all Q^2 bins. Only statistical uncertainties are included in the data points. Systematic uncertainties are small compared to statistical errors and are not shown. The line represents the single Breit-Wigner fit.

a small nonresonant contribution to the cross section, and none is needed here. The simple shape describes the low W region well, but there are deviations for $W > 1.6$ GeV, presumably because of interference between $S_{11}(1535)$, $S_{11}(1650)$, and nonresonant processes. Although the higher mass resonance is very near to the state we seek to describe, all analyses [9] find a very small ηN branching fraction for $S_{11}(1650)$. Therefore, we restrict the fit to W values less than 1.6 GeV. Two previous experiments [16,17] performed longitudinal/transverse separations in the late 1970s. Their results are consistent with no longitudinal component, albeit with large uncertainties. For the results presented here, the different beam energies have insufficient overlap in W and Q^2 to separate these components. Under the assumption that the cross section is dominated by a single resonance and that $S_{\frac{1}{2}}$ is small, we can relate the $A_{\frac{1}{2}}$ to the peak cross sections extracted from the fit [see Eqs. (4) and(5)]:

$$A_{\frac{1}{2}}(Q^2) = \left[\frac{W_R \Gamma_R}{2 m_p b_\eta}\sigma(W_R, Q^2)\right]^{1/2}. \qquad (12)$$

Consistent with Armstrong *et al.* [19], a value of the full width of 150 MeV and an $S_{11} \to \eta N$ branching ratio of 0.55 were used. The results of this determination of $A_{\frac{1}{2}}$ are shown in Fig. 4 along with some previous results converted to be consistent with our choice of Γ_R and b_η. The extracted values for $A_{1/2}$ for this experiment are also listed in Table IV. The precise normalization of $A_{\frac{1}{2}}$ depends on the choice of parameters for the contributing resonances, which are, as yet, not well determined. For instance, using the range of values listed in PDG for Γ_R and b_η leads to an 11%

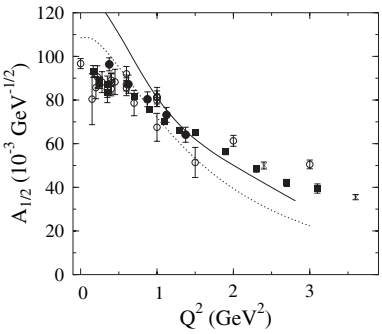

FIG. 4. Extracted values for $A_{\frac{1}{2}}$ for $\gamma p \to S_{11}(1535)$ transition for this experiment (filled squares). There are overlapping data points at $Q^2 = 0.25$ and 0.35 GeV^2 coming from data taken with two different magnetic field settings. Filled circles show results from our previous smaller data set [21]. JLab results from Armstrong *et al.* [19] are shown as crosses. The open circles are results from earlier publications [11,13,14,16–18]. All results have been converted to represent a common width and branching ratio for $S_{11}(1535) \to \eta p$. The theoretical models are from constituent quark models of Capstick and Keister [2] (solid line) and Aiello, Gianinni, and Santopinto [41] (dotted curve).

systematic uncertainty on $A_{\frac{1}{2}}$. While these uncertainties affect the *absolute* value of $A_{\frac{1}{2}}$, the *shape* of the Q^2 dependence is much better determined. More detailed understanding of this state is required to better determine absolute values of $A_{\frac{1}{2}}$ and estimate the model dependence of those values. Using the choice of Γ and b_η described above, our extracted values are consistent with the previous values at low Q^2 [13,14,16,17], but with smaller uncertainties. At high Q^2, there is moderate disagreement between the previously published results of Brasse *et al.* [18] (at $Q^2 = 2.0$ and 3.0 GeV^2) and Armstrong *et al.* [19] (at 2.4 and 3.6 GeV^2). Our results match up nicely with Armstrong *et al.* and provide a precise determination of the shape of the Q^2 dependence of $A_{\frac{1}{2}}$ from low Q^2 up to their high Q^2 determinations.

TABLE IV. Extracted values for $A_{\frac{1}{2}}$ for $\gamma p \to S_{11}(1535)$ transition for this experiment. In addition to the systematic uncertainties shown, there is also an 11% uncertainty due to the current uncertainty in Γ_R, W_R, and b_η.

Q^2 (GeV^2)	$A_{1/2}$ ($10^{-3}/\sqrt{\text{GeV}}$)
0.165	$93.1 \pm 2.7 \pm 0.8$
0.25	$88.6 \pm 1.9 \pm 0.4$
0.35	$83.5 \pm 2.3 \pm 0.7$
0.25	$87.7 \pm 0.9 \pm 1.4$
0.35	$86.9 \pm 0.9 \pm 0.5$
0.7	$81.5 \pm 1.1 \pm 0.4$
0.9	$75.6 \pm 1.1 \pm 0.3$
1.1	$70.0 \pm 1.2 \pm 0.4$
1.3	$66.1 \pm 1.3 \pm 0.3$
1.5	$65.1 \pm 1.4 \pm 0.5$
1.9	$56.2 \pm 1.3 \pm 0.3$
2.3	$48.4 \pm 1.5 \pm 0.3$
2.7	$42.0 \pm 1.6 \pm 0.3$
3.1	$39.4 \pm 2.1 \pm 0.5$

TABLE V. Binning details for the differential cross sections. For each Q^2 bin, we show the minimum and maximum values of Q^2, the energy of the electron beam for the data set, the maximum value of W probed, and the bin width in $\cos\theta^*$. The W bin widths in all cases were 20 MeV, while the ϕ^* bins were 30° wide.

Q^2_{min} (GeV^2)	Q^2_{max} (GeV^2)	E_{beam} (GeV)	W_{max} (GeV)	$\Delta \cos\theta^*$
0.2	0.4	1.5	1.60	0.2
0.6	1.0	2.5	1.80	0.2
1.0	1.4	2.5	1.74	0.2
1.3	2.1	4.0	2.00	0.4
2.1	2.9	4.0	1.92	0.4

The literature has various theoretical calculations of the photocoupling amplitude within the constituent qark model (CQM). Matching the slow falloff with Q^2 has been difficult. We show two recent calculations [2,41]. Aiello, Giannini, and Santopinto [41] use a hypercentral CQM and emphasize the importance of the three-body quark force. Although this prediction gives the best agreement with our data of all the calculations, it falls off more rapidly with Q^2 than the data. The Capstick and Keister calculation [2] starts with the more traditional CQM but uses relativistic dynamics in a light-front framework. Although the two calculations use different approaches, the CQM is not well defined, and many other results are given in the literature.

B. Differential cross sections

For larger bins in W and Q^2 (see Table V), we extract differential cross sections vs center-of-mass scattering angles of the η ($\cos\theta^*$ and ϕ^*). Each bin is labeled by its centroid. Results from this experiment are tabulated in the CLAS database [40]. For the $Q^2 = 0.8$ GeV^2 bin, Fig. 5 shows sample cross sections for four W bins. The first two W bins, $W = 1.52$ and 1.54 GeV, are at the peak of the $S_{11}(1535)$ resonance. They show a dominant isotropic component due to the $S_{11}(1535) \to \eta p$ process, but deviations from isotropy can be seen, especially at large ϕ^*. By $W = 1.66$ GeV, the nonisotropy is quite evident. The cross section falls monotonically as a function of $\cos\theta^*$, with the cross section for forward η production consistent with zero. As W increases, this feature changes dramatically. At $W = 1.72$ GeV, the forward-backward asymmetry of the distributions has reversed, with forward η production favored, while backward production is close to zero.

The η-MAID model [29], based on the MAID formalism [30], has been developed for η electro- and photoproduction. This is an isobar model using a relativistic Breit-Wigner W dependence with form factors. Eight PDG 3$*$ and 4$*$ resonances of mass less than 1.8 GeV and nonresonant processes are included at the amplitude level. They fit the photoproduction data [11,12,42] and the Q^2 dependence of the total cross section from electroproduction data [19,21] in

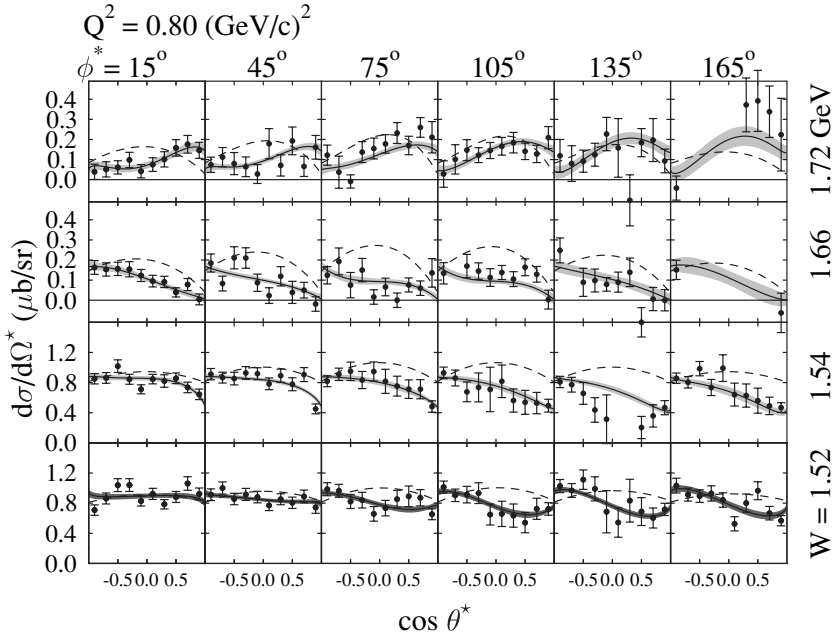

FIG. 5. Sample differential cross sections for $\gamma_v p \to \eta p$ in the c.m. frame for $Q^2 = 0.8$ GeV^2 and selected W bins. Values for ϕ_η^* symmetric about 180° have been averaged. [No information is lost this way; see Eq. (2).] Solid lines with an error band correspond to the response function fit described in the text. Dashed lines correspond to the calculation of η-MAID [29].

the $S_{11}(1535)$ region. The results of a calculation implementing this model are included in Fig. 5. These calculations roughly match the observed cross sections. However, the angular dependence predicted by η-MAID does not agree with our data at W above the $S_{11}(1535)$ region. The model was not fit to the differential cross sections of our previous work and the Q^2 dependence of the higher mass resonances, e.g., $D_{15}(1675)$, was taken from a quark model calculation rather than from data.

For each W and Q^2 bin, the differential cross sections are fit to a form that comes from an expansion of the response functions from Eq. (2) in terms of associated Legendre polynomials $P_\ell^m(\cos\theta_\eta^*)$, that is,

$$\frac{d^2\sigma}{d\Omega_\eta^*} = \sum_{\ell=0}^{\infty} A_\ell P_\ell^0(\cos\theta_\eta^*) + \sum_{\ell=1}^{\infty} B_\ell P_\ell^1(\cos\theta_\eta^*)\cos\phi_\eta^* + \sum_{\ell=2}^{\infty} C_\ell P_\ell^2(\cos\theta_\eta^*)\cos 2\phi_\eta^*. \quad (13)$$

The parameters B_ℓ, B_ℓ, and C_ℓ depend on Q^2, W, and ϵ. They represent bilinear sums over contributing multipole amplitudes. Truncating to $\ell \leqslant 3$, we determined the parameters in Eq. (13) by a fit to the data. This truncation is motivated by three effects. (i) The lightest known N^* resonance with $\ell > 3$ is the $G_{17}(2190)$; if the dominant effects on the differential cross section arise from interference with the dominant $\ell = 0$ partial wave, terms above $l = 3$ should be negligible. (ii) Fits to the η-MAID predicted cross sections yield negligible contributions for terms higher than $\ell = 3$. (iii) Good fits to the data are obtained with the truncated sum.

Results are shown vs W in Figs. 6–8. The quoted uncertainties contain both statistical and systematic uncertainties. We repeated the fit taking into account shifts in the cross section for each of the sources of systematic uncertainty studied in Sec. III. The total systematic uncertainty on the extracted parameters is the sum in quadrature of all individual sources. We normalize our fitted A_1, A_2, etc., to the isotropic term A_0 in order to more clearly show the W and Q^2 dependence of the shape of the differential cross section. For the ratios, the resulting uncertainty is dominated by the uncertainty on the numerators.

The isotropic component $A_0 = \sigma_{\rm tot}/4\pi$ shows the same features as the angle-integrated cross sections: a dominant peak from the $S_{11}(1535)$ with additional structure above $W = 1.6$ GeV. The other prominent term in the fit is A_1, which represents the slope of the differential cross section vs $\cos\theta_\eta^*$. A structure in the W dependence of A_1 was first seen in our previous publication [21] and is also seen by the GRAAL photoproduction experiment [42]. By examining the ratio A_1/A_0 in the new data, we can study this structure in more detail. Two features stand out in this ratio:

(i) The ratio A_1/A_0 is large and makes a rapid change from negative to positive values at $W \approx 1.7$ GeV.
(ii) This structure is roughly independent of Q^2 up to 2.5 GeV^2.

The simplest description for A_1 is in terms of interference between S and P waves. In that case, the rapid change in A_1 between $W = 1.66$ and 1.72 GeV could be caused by one of the waves passing through a resonance. There are two P-wave resonances in this region, $P_{11}(1710)$ and $P_{13}(1720)$. The former is rated 3∗ by the PDG [9], but its properties are very difficult to extract from data and is therefore controversial [43]. The latter is rated 4∗, but is also poorly understood [10]. Fits to CLAS $\pi^+\pi^-$ electroproduction data [23] provided evidence that the existing baryon structure at $W \sim 1.7$ GeV should be changed. Their fits prefer either a greatly reduced ρN decay branch for the existing $P_{13}(1720)$ resonance or a new $\frac{3}{2}^+$ state. In the present data, we cannot couple to a $T = 3/2$ state

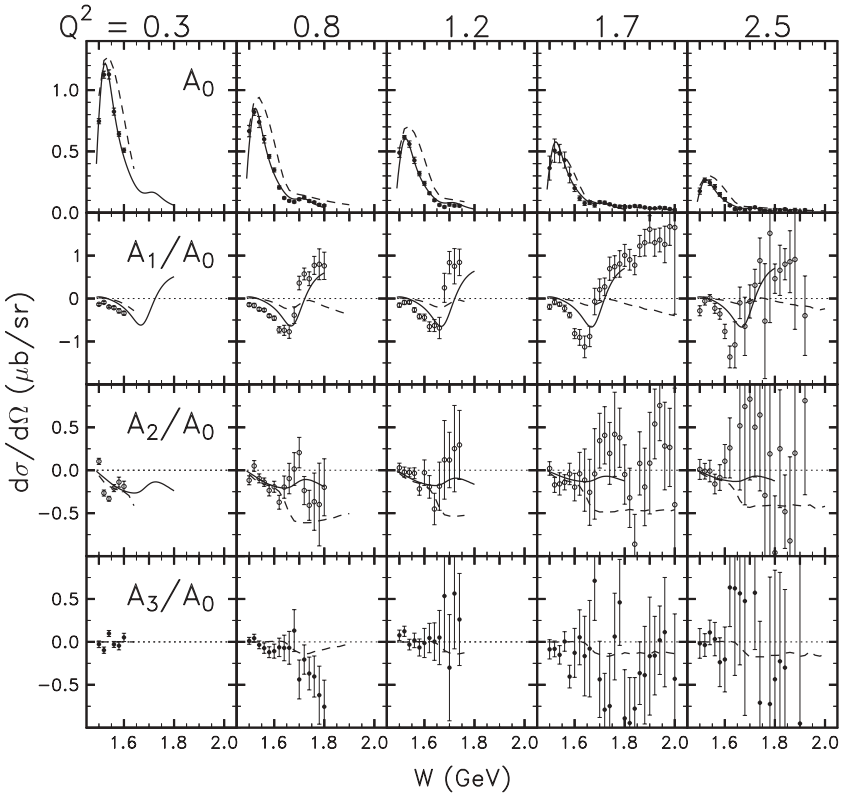

FIG. 6. Results from fitting the angular distribution data of this experiment to Eq. (13). Coefficients of the ϕ^* independent terms are shown, i.e., those that contribute to $\sigma_T + \epsilon\sigma_L$. Contributions from both statistical and systematic sources are displayed. The dashed line is the η-MAID prediction [29]; solid line is a four resonance fit to these terms.

and are unable to distinguish between P_{11} and P_{13} states; we choose to use only a P_{11} state. If one describes the cross section using *only* S_{11} and P_{11} partial waves, then

$$\frac{A_1}{A_0} = \frac{2\Re(E_{0+}^* M_{1-})}{|E_{0+}|^2 + |M_{1-}|^2}. \tag{14}$$

In this case, the rapid shift from backward to forward peaked cross sections would be due to a rapid change in the relative phase of the E_{0+} and M_{1-} multipoles, because one of them is passing through resonance. The observation that this structure in A_1/A_0 is approximately Q^2 independent would then imply that S_{11} and P_{11} partial waves have a similar Q^2 dependence.

The values of B_ℓ shown in Fig. 7 are consistent with zero. These parameters measure the σ_{LT} component of $\frac{d\sigma}{d\Omega}$, indicating that longitudinal amplitudes are not significant for this reaction (as was assumed in Sec. IV A). The C_l parameters

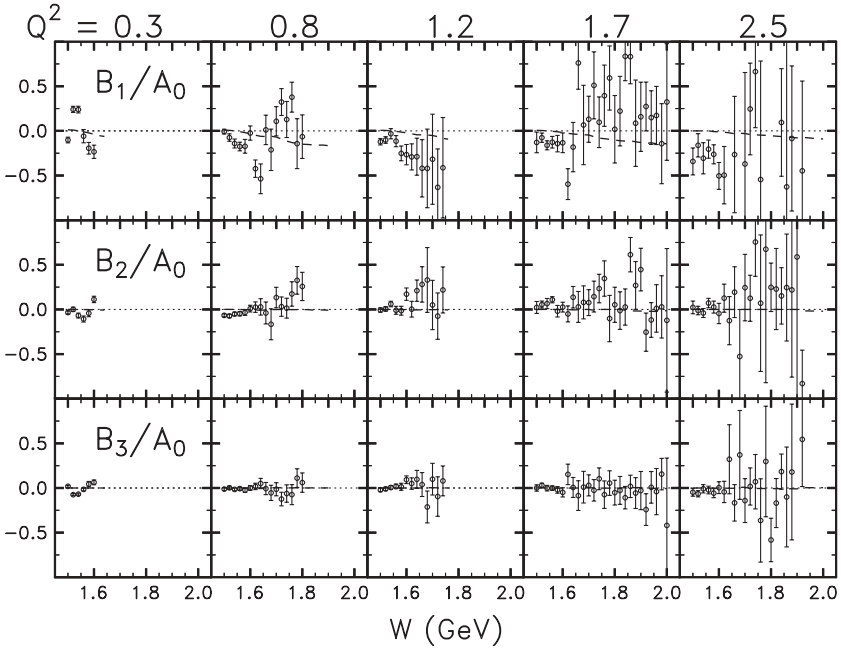

FIG. 7. Same as Fig. 6, but showing the parameters corresponding to σ_{LT}. For the four resonance fit, these parameters are all zero.

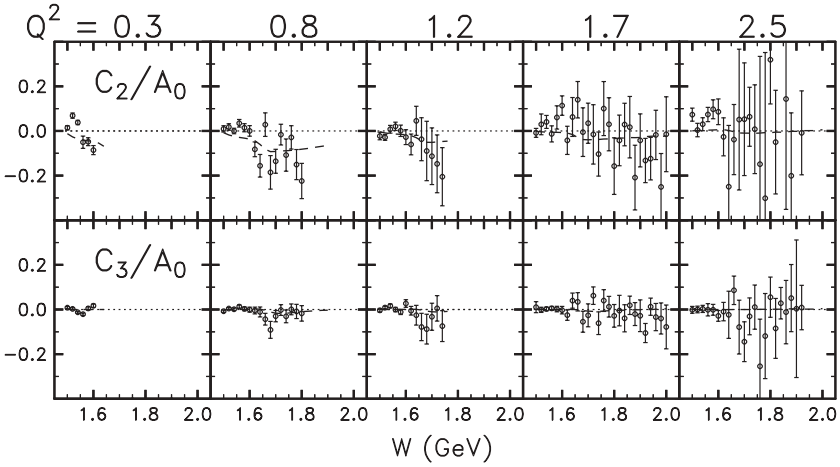

FIG. 8. Same as Fig. 6, but showing the parameters corresponding to σ_{TT}. For the four resonance fit, these parameters are all zero.

in Fig. 8 measure the σ_{TT} component of $\frac{d\sigma}{d\Omega}$. They are small, indicating that the $A_{3/2}$ components are also small for these values of Q^2.

To better understand the content of the η-MAID model, we also fit the parameters in Eq. (13) to the predicted cross sections from that model. The extracted parameters are also included in Figs. 6–8 as dashed lines. The prediction has a broader S_{11} peak than is seen in our data. Some structure is predicted in A_1 arising from the $P_{11}(1710)$, but the size of this effect is not nearly enough to match our data. At high W, η-MAID predicts a negative A_1 in contrast to the significant positive value we observe. The model value of $b_{\eta N}$ for $P_{11}(1710)$ is much larger than the PDG value. Our data indicate the model value is incorrect. η-MAID contains many sources of D-wave contributions: $D_{13}(1520)$, $D_{13}(1700)$, and $D_{15}(1675)$ in addition to nonresonant amplitudes. This produces a value for A_2/A_0 that matches our data for $W < 1.6$ GeV, where the $D_{13}(1520)$ is the leading contribution. At larger W, agreement is poor. The model value of $b_{\eta N}$ for $D_{15}(1675)$ is much larger than the PDG value; our data indicate this is incorrect. The prediction for A_3/A_0 is near zero, as are our measurements.

Predictions for the σ_{LT} and σ_{TT} terms are consistent with our measurements. C_2 is the only term that is not negligible in η-MAID for our values of Q^2. It arises from the $A_{3/2}$ amplitudes of the D-wave resonances interfering with the larger S-wave amplitude. Our data agree with this general trend, but the effect is small compared to the uncertainties.

To gain further understanding of the resonance content of our data, we did an additional fit to the differential cross section data using relativistic Breit-Wigner resonances according to Eqs. (7)–(10). We fit the extracted parameters, up to $W = 1.8$ GeV, to a sum of four amplitudes for the following resonances: $S_{11}(1525)$, $S_{11}(1650)$, $P_{11}(1710)$, and $D_{13}(1520)$. This set of resonances was determined empirically as the minimal set required to fit the general features of our data. Although the properties of $P_{11}(1710)$ are very uncertain, it is an important contributor to this fit. We label it as P_{11}, but we cannot distinguish between P_{11} and $P_{13}(1720)$ in our data set; specifically, a P_{13} resonance would also give a rapid energy dependence in either A_2 or C_2 which we are unable to exclude with current statistical accuracy. Only the transverse response function σ_T is modeled, i.e., the A_i parameters. For the resonances with small contributions [$S_{11}(1650)$ and $D_{13}(1520)$], we fixed the resonance parameters to values obtained elsewhere. Masses and widths were set to average values from the Particle Data Group. For the $D_{13}(1520)$, we used the Q^2 dependence of η-MAID. Following the assumption of the single quark transition model [44], the ratio of the strength of the $S_{11}(1650)$ to that of the $S_{11}(1535)$ was taken to be independent of Q^2. Motivated by the Q^2 independence of A_1/A_0 in our data, we assumed the $P_{11}(1710)$ had the same Q^2 dependence as the S_{11} states. This left 12 variables in the fit: the masses and widths of the $S_{11}(1535)$ and $P_{11}(1710)$, the relative strengths of the $S_{11}(1650)$ and $P_{11}(1710)$ to that of the $S_{11}(1535)$, an overall strength of the $D_{13}(1520)$, and the absolute strength of the $S_{11}(1535)$ in each of the five Q^2 bins. We view this as a simple fit. Our results should not be interpreted as a precise determination of resonance parameters, but rather as an indication of the dominant components needed in any future theoretical work.

The results of this fit are also shown in Fig. 6. The fit yields a reasonable, though not perfect description of our data. The isotropic term A_0 is described by the dominant $S_{11}(1535)$ peak, modified by the smaller $S_{11}(1650)$. The deviation from a simple Breit-Wigner is described as a combination of destructive interference between the $S_{11}(1535)$ and $S_{11}(1650)$, and a small contribution from the $P_{11}(1710)$. Including the $S_{11}(1650)$ results in an extracted value of $A_{\frac{1}{2}}$ for the $S_{11}(1535)$ which is 7% higher than that obtained with a single Breit-Wigner. The fitted width of the $P_{11}(1710)$ is 100 MeV, which is consistent with the central (but very uncertain) PDG value. We cannot isolate the $P_{11}(1710)$ photocoupling from that state's branching ratio into ηp; we can only quote a ratio of ξ values [Eq. (6)]. The extracted value of ξ_{1710}/ξ_{1535} is 0.22, which is about twice as large as in η-MAID, and nearly an order of magnitude larger than that extracted from parameters of the $P_{11}(1710)$ in the PDG. The $D_{13}(1520)$ primarily affects the quadratic term A_2. Including this resonance is enough to give a reasonable description of the W dependence of A_2. Our data do not require significant contributions from higher D-wave states present in the η-MAID model.

We fit the structure in A_1/A_0 with a smooth S wave and a rapidly changing P wave. One could also describe this structure in terms of a new S-wave resonance interfering

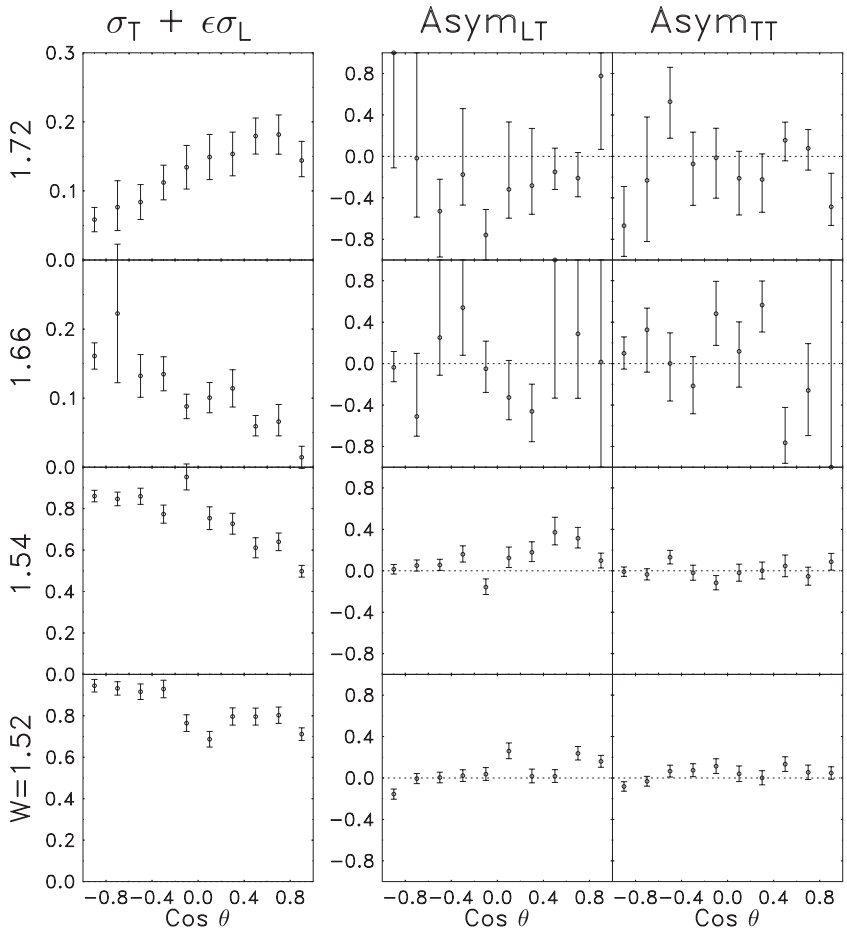

FIG. 9. Extracted values for $\sigma_T + \epsilon\sigma_L$, Asym_{LT}, and Asym_{TT} as a function of $\cos\theta^*$ for four selected W bins with $Q^2 = 0.8\ \mathrm{GeV}^2$.

with the P-wave component as in the model of Saghai and Li [45]. However, the amplitudes for the new resonance and the P-wave component must both fall off slowly with Q^2 to reproduce the data.

We also fit the ϕ dependence of the differential cross sections directly to Eq. (2) in order to obtain $\sigma_T + \epsilon\sigma_L$, σ_{LT}, and σ_{TT} as a function of W, Q^2, and $\cos\theta^*$. We choose to fit the ϕ^* dependence in terms of the parallel/perpendicular asymmetry (Asym_{TT}) and the parallel/anti-parallel asymmetry (Asym_{LT}).

$$\mathrm{Asym}_{TT} = \frac{\sigma_{||} - \sigma_{\perp}}{\sigma_{||} + \sigma_{\perp}}, \tag{15}$$

where

$$\sigma_{||} = \tfrac{1}{2}\left(\sigma(\phi = 0) + \sigma(\phi = \pi)\right) \tag{16}$$

and

$$\sigma_{\perp} = \tfrac{1}{2}\left(\sigma(\phi = \pi/2) + \sigma(\phi = 3\pi/2)\right). \tag{17}$$

$$\mathrm{Asym}_{LT} = \frac{\sigma(\phi = 0) - \sigma(\phi = \pi)}{\sigma(\phi = 0) + \sigma(\phi = \pi)}. \tag{18}$$

For photoproduction, σ_L and σ_{LT} do not contribute. A common polarization parameter is the parallel/perpendicular asymmetry, Σ. It is defined by $\mathrm{Asym}_{TT} = \epsilon\Sigma$; note also that $\Sigma = \sigma_{TT}/\sigma_T$. In electroproduction, the possible presence of a longitudinal term makes the relationships more complicated:

$$\mathrm{Asym}_{TT} = \frac{\epsilon\sigma_{TT}}{\sigma_T + \epsilon\sigma_L}, \tag{19}$$

$$\mathrm{Asym}_{LT} = \frac{\sqrt{2\epsilon(\epsilon+1)}\sigma_{LT}}{\sigma_T + \epsilon\sigma_L + \epsilon\sigma_{TT}}. \tag{20}$$

The data were analyzed in terms of these three response function combinations. A treatment of systematic uncertainties similar to that used for differential cross sections was applied. Figure 9 shows the values extracted from these fits for the same W and Q^2 shown in Fig. 5. Error bars display the systematic and statistical uncertainties. The quantity $\sigma_T + \epsilon\sigma_L$ shows the same features we discussed earlier. The values for Asym_{TT} are consistent with zero in all distributions, but the size of the estimated error bars are a strong function of W. For $W > 1.6$, the total cross section is smaller than where the S_{11} resonance dominates. Extraction of meaningful values for the ϕ dependence in this manner is therefore difficult.

V. CONCLUSIONS

Our extractions of $A_{\frac{1}{2}}$ for the excitation of the $S_{11}(1535)$ cover a large range and match up well with Armstrong's results [19] at higher Q^2. It should be noted again that there are significant model dependencies on describing the mass, width, and branching ratio into ηp. These uncertainties lead

to significant systematic uncertainties on the absolute scale of $A_{\frac{1}{2}}$. These uncertainties are common to all points currently determined, so the shape of the distribution is well determined. It becomes a significant challenge for theory to reproduce this shape. No existing model is able to describe the full range.

Knowledge of the N^* resonances in the region $W\sim$ 1700 MeV is presently weak, because the quality of older $\pi N \to \pi\pi N$ and $\pi N \to \eta N$ data is poor. The coupling of known P-wave resonances to ηN is thought to be very small. In this experiment, rapid energy dependence in the strength in the P-wave for coupling to ηN final states is found. With a simple resonance model, we are able to describe these data with significant coupling of a P-wave resonance to ηN. As with $S_{11}(1535)$, the falloff of this coupling must be very slow.

Although we can describe our measurements in terms of the $P_{11}(1710)$, we cannot distinguish between that or the $P_{13}(1720)$ with these data. Either resonance could produce the effect seen in A_1/A_0. The $P_{11}(1710)$ is more poorly understood than the $P_{13}(1720)$, so it is easier to accommodate our data by altering the partial widths of the P_{11} rather than the P_{13}. A large P_{13} could also produce effects in other terms. For instance, interference with a D wave would give a small contribution to $A_{\frac{3}{2}}$, but it would not be significant compared to our uncertainties. A P_{13} resonance would have an $A_{\frac{3}{2}}$ photo-excitation as well as $A_{\frac{1}{2}}$. Our determination of A_1/A_0 is sensitive to the $A_{\frac{1}{2}}$ amplitude; a significant $A_{\frac{3}{2}}$ amplitude could also lead to large effects in σ_{TT}.

Evidence for possible alterations in N^* P-wave resonances at masses of about 1.7 GeV is accumulating. In addition to what is found in this experiment, double-pion production experiments in this same mass range [23,46] are also unable to be described with models using existing information. Since different models are used to describe the different data sets, it is important to use a common model to describe the combined measurements from these (and other) reactions. Such a program may allow us to accurately determine the properties of the P-wave resonances in this region.

ACKNOWLEDGMENTS

We acknowledge the outstanding efforts of the staff of the Accelerator and the Physics Divisions at JLab that made this experiment possible. This work was supported in part by the U.S. Department of Energy, the National Science Foundation, the Istituto Nationale di Fisica Nucleare, the French Centre National de la Recherche Scientifique, the French Commissariat à l'Energie Atomique, and the Korea Science and Engineering Foundation. Jefferson Science Associates (JSA) operates the Thomas Jefferson Science Facility for the U.S. Department of Energy under Contract DE-AC05-06OR23177.

[1] W. Konen and H. J. Weber, Phys. Rev. D **41**, 2201 (1990).
[2] S. Capstick and B. D. Keister, Phys. Rev. D **51**, 3598 (1995).
[3] F. E. Close and Z.-P. Li, Phys. Rev. D **42**, 2194 (1990).
[4] C. Alexandrou, P. de Forcrand, H. Neff, J. W. Negele, W. Schroers, and A. Tsapalis, Phys. Rev. Lett. **94**, 021601 (2005).
[5] J. M. Zanotti, D. B. Leinweber, A. G. Williams, and J. B. Zhang, Nuc. Phys. Proc. Suppl. **129**, 287 (2004).
[6] S. Basak *et al.* (Lattice Hadron Physics Collaboration), PoS **LAT2006**, 197 (2006); arXiv:hep-lat/0609072.
[7] B. Krusche and S. Schadmand, Prog. Part. Nucl. Phys. **51**, 399 (2003).
[8] V. D. Burkert and T. S. H. Lee, Int. J. Mod. Phys. E **13**, 1035 (2004).
[9] W.-M. Yao, C. Amsler, D. Asner, R. Barnett, J. Beringer, P. Burchat, C. Carone, C. Caso, O. Dahl, G. D'Ambrosio *et al.* (Particle Physics Group), J. Phys. G **33**, 1 (2006).
[10] T. P. Vrana, S. A. Dytman, and T. S. H. Lee, Phys. Rep. **328**, 181 (2000).
[11] B. Krusche *et al.*, Phys. Rev. Lett. **74**, 3736 (1995).
[12] J. Ajaka *et al.*, Phys. Rev. Lett. **81**, 1797 (1998).
[13] P. S. Kummer *et al.*, Phys. Rev. Lett. **30**, 873 (1973).
[14] U. Beck *et al.*, Phys. Lett. **B51**, 103 (1974).
[15] J. C. Alder *et al.*, Nucl. Phys. **B91**, 386 (1975).
[16] F. W. Brasse *et al.*, Nucl. Phys. **B139**, 37 (1978).
[17] H. Breuker *et al.*, Phys. Lett. **B74**, 409 (1978).
[18] F. W. Brasse *et al.*, Z. Phys. C **22**, 33 (1984).
[19] C. S. Armstrong *et al.* (Jefferson Lab E94014), Phys. Rev. D **60**, 052004 (1999).
[20] M. Ungaro *et al.* (CLAS Collaboration), Phys. Rev. Lett. **97**, 112003 (2006).
[21] R. Thompson *et al.* (CLAS Collaboration), Phys. Rev. Lett. **86**, 1702 (2001).
[22] B. A. Mecking *et al.* (CLAS Collaboration), Nucl. Instrum. Methods A **503**, 513 (2003).
[23] M. Ripani *et al.* (CLAS Collaboration), Phys. Rev. Lett. **91**, 022002 (2003).
[24] V. Crede *et al.* (CB-ELSA Collaboration), Phys. Rev. Lett. **94**, 012004 (2002).
[25] L. N. Hand, Phys. Rev. **129**, 1834 (1963).
[26] G. Chew, M. Goldberger, F. Low, and Y. Nambu, Phys. Rev. **106**, 1345 (1957).
[27] Thomas G. Trippe *et al.* (Particle Data Group), Rev. Mod. Phys. **48**, S1 (1976).
[28] R. A. Arndt, W. J. Briscoe, I. I. Strakovsky, and R. L. Workman, Phys. Rev. C **66**, 055213 (2002).
[29] W.-T. Chiang, S.-N. Yang, L. Tiator, and D. Drechsel, Nucl. Phys. **A700**, 429 (2002).
[30] D. Drechsel, O. Hanstein, S. S. Kamalov, and L. Tiator, Nucl. Phys. **A645**, 145 (1999).
[31] M. Dugger *et al.* (CLAS Collaboration), Phys. Rev. Lett. **89**, 222002 (2002).
[32] I. G. Aznauryan, V. D. Burkert, G. V. Fedotov, B. S. Ishkhanov, and V. Mokeev, Phys. Rev. C **72**, 045201 (2005).
[33] M. Benmerrouche, N. C. Mukhopadhyay, and J. F. Zhang, Phys. Rev. D **51**, 3237 (1995).
[34] B. Krusche, N. Mukhopadhyay, J. Zhang, and M. Benmerrouche, Phys. Lett. **B397**, 171 (1997).
[35] G. Knochlein, D. Drechsel, and L. Tiator, Z. Phys. A **352**, 327 (1995).
[36] J. Blatt and V. Weisskopf, *Theoretical Nuclear Physics* (Dover, New York, 1991).

[37] R. Ent, B. Fillipone, N. Makins, R. Milner, T. O'Neill, and D. Wasson, Phys. Rev. C **64**, 054610 (2001).
[38] L. Mo and Y. Tsai, Rev. Mod. Phys. **41**, 205 (1969).
[39] GEANT Detector Description and Simulation Tool, CERN, Geneva, w5013 (1993).
[40] Physics database of CLAS collaboration, http://clasweb.jlab.org/physicsdb.
[41] M. Aiello, M. M. Giannini, and E. Santopinto, J. Phys. G **24**, 753 (1998).
[42] F. Renard *et al*. (GRAAL Collaboration), Phys. Lett. **B528**, 215 (2002).
[43] R. A. Arndt, Y. I. Azimov, M. V. Polyakov, I. I. Strakovsky, and R. L. Workman, Phys. Rev. C **69**, 035208 (2004).
[44] A. Hey and J. Weyers, Phys. Lett. **B48**, 69 (1974).
[45] B. Saghai and Z.-P. Li, Eur. Phys. J. A **11**, 217 (2001).
[46] Y. Assafiri *et al*., Phys. Rev. Lett. **90**, 222001 (2003).